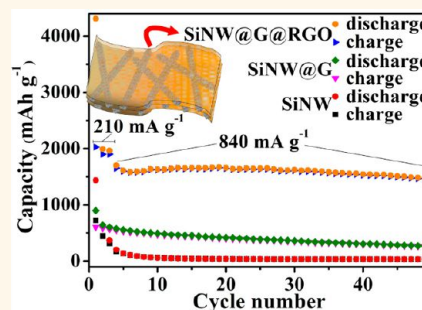


# Adaptable Silicon–Carbon Nanocables Sandwiched between Reduced Graphene Oxide Sheets as Lithium Ion Battery Anodes

Bin Wang,<sup>†</sup> Xianglong Li,<sup>†,\*</sup> Xianfeng Zhang,<sup>†</sup> Bin Luo,<sup>†</sup> Meihua Jin,<sup>†</sup> Minghui Liang,<sup>†</sup> Shadi A. Dayeh,<sup>‡</sup> S. T. Picraux,<sup>§</sup> and Linjie Zhi<sup>†,\*</sup>

<sup>†</sup>National Center for Nanoscience and Technology, Beijing 100190, P. R. China, <sup>‡</sup>Department of Electrical and Computer Engineering, University of California San Diego, La Jolla, California 92093, United States, and <sup>§</sup>Center for Integrated Nanotechnologies, Materials Physics and Applications Division, Los Alamos National Laboratory, Los Alamos, New Mexico 87545, United States

**ABSTRACT** Silicon has been touted as one of the most promising anode materials for next generation lithium ion batteries. Yet, how to build energetic silicon-based electrode architectures by addressing the structural and interfacial stability issues facing silicon anodes still remains a big challenge. Here, we develop a novel kind of self-supporting binder-free silicon-based anodes *via* the encapsulation of silicon nanowires (SiNWs) with dual adaptable apparels (overlapped graphene (G) sheaths and reduced graphene oxide (RGO) overcoats). In the resulted architecture (namely, SiNW@G@RGO), the overlapped graphene sheets, as adaptable but sealed sheaths, prevent the direct exposure of encapsulated silicon to the electrolyte and enable the structural and interfacial stabilization of silicon nanowires. Meanwhile, the flexible and conductive RGO overcoats accommodate the volume change of embedded SiNW@G nanocables and thus maintain the structural and electrical integrity of the SiNW@G@RGO. As a result, the SiNW@G@RGO electrodes exhibit high reversible specific capacity of 1600 mAh g<sup>-1</sup> at 2.1 A g<sup>-1</sup>, 80% capacity retention after 100 cycles, and superior rate capability (500 mAh g<sup>-1</sup> at 8.4 A g<sup>-1</sup>) on the basis of the total electrode weight.



**KEYWORDS:** silicon nanowire · graphene · adapting · lithium ion battery

The development of rechargeable lithium-ion batteries (LIBs) with high energy density, high-rate capability, and excellent cycling performance is critically important for automotive and stationary energy storage applications such as electric vehicles, power tools, multifunctional electronic devices, and communication equipments, as well as renewable energy integration.<sup>1,2</sup> From the viewpoint of electrode materials, silicon (Si) is one of the most promising candidates as an anode material for LIBs due to its abundance in nature, appropriately low working potential, and highest known theoretical specific capacity of ~4200 mAh g<sup>-1</sup> which is more than 10 times higher in comparison to that of commercialized graphite anodes.<sup>3–5</sup> However, silicon experiences a dramatic volume change (>300%) during the lithiation and delithiation processes,<sup>6</sup> leading to not only severe pulverization and subsequent electrical

disconnection from the current collector, but also continual formation of so-called solid electrolyte interphase (SEI) on the silicon surfaces newly exposed to the electrolyte. Both effects result in the performance degradation of silicon, producing two impending challenges for the development of Si-based anodes, namely, the stabilization of Si structures and the engineering of their interfaces with electrolyte.<sup>5</sup> In this context, remarkable improvements in the electrochemical performance of silicon have been achieved through diverse strategies specifically for engineering active material, current collector, binder and/or their interface.<sup>7–24</sup> While the nanoscale structural modulation<sup>3,7–9</sup> of Si can improve its mechanical integrity during charge/discharge cycling, the shielding of nanostructured Si with a second phase is further considered one of the most promising tactics for simultaneously dealing with both challenges. To achieve this

\* Address correspondence to  
zhilj@nanoctr.cn;  
lixl@nanoctr.cn.

Received for review November 8, 2012  
and accepted January 2, 2013.

Published online January 02, 2013  
10.1021/nn3052023

© 2013 American Chemical Society

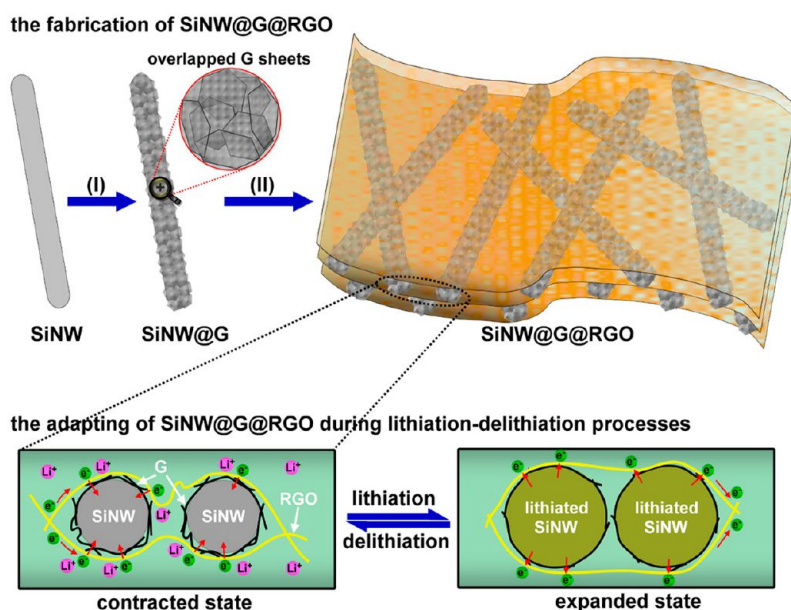


**Figure 1.** Schematic of the fabrication (upper panel) and adapting (lower panel) of SiNW@G@RGO. The fabrication process mainly includes (I) chemical vapor deposition (CVD) growth of overlapped graphene sheets on as-synthesized silicon nanowires (SiNWs) to form SiNW@G nanocables, and (II) vacuum filtration of an aqueous SiNW@G-graphene oxide (GO) dispersion followed by thermal reduction. The resulting SiNW@G@RGO can transform between an expanded state and a contracted state during lithiation–delithiation cycles, thus enabling the stabilization of the silicon material.

shielding, a wide variety of silicon nanostructures confined with organic/inorganic substances as the mechanically rigid and spatially sealed shells/sheaths have been investigated such as amorphous carbon-coated Si nanowires<sup>10</sup>/nanotubes<sup>11,12</sup>/particles,<sup>8,13,14</sup> amorphous carbon shell-sheltered Si yolks,<sup>15</sup> thick nitrogen-doped graphitic layer-sheathed Si nanowires,<sup>16</sup> poly(3,4-ethylenedioxythiophene) (PEDOT)-coated Si nanowires,<sup>17</sup> electrospun carbon nanofiber-protected Si nanoparticles,<sup>18,19</sup> double-shell Si@SiO<sub>2</sub>@C composites,<sup>20,21</sup> SiO<sub>x</sub>-covered Si nanotubes,<sup>5</sup> and Al<sub>2</sub>O<sub>3</sub>-coated Cu–Si nanocable arrays.<sup>22</sup> Given the absence of void space inside these rigid and sealed shells/sheaths, however, these shells/sheaths are prone to disintegrate due to the huge volume expansion of interior silicon,<sup>15,19</sup> which can lead to unstable electrode structures and incur the volume change-related problems. As an alternative, graphene<sup>25</sup> and/or its derivatives (e.g., reduced graphene oxide<sup>26</sup>) are employed as robust and elastic substances to encapsulate silicon nanoparticles, as well as show potential for advancing Si-based anodes.<sup>27,28</sup> Yet, the simple combination of Si nanoparticles with graphene sheets indeed constructs open channels for the direct contact of silicon with the electrolyte, which can degrade the cycling performance.

Consistent with a recent commentary<sup>29</sup> highlighting the importance of engineering the interactions between individual components of a system, here, we develop a novel kind of adaptable self-supporting binder-free silicon-based anodes. As shown in Figure 1, silicon nanowires (SiNWs), as a representative model, are sheathed with overlapped graphene (G) sheets to

form core–sheath nanocables (SiNW@G) (step I), and are in turn sandwiched between reduced graphene oxide (RGO) sheets (step II), thus forming RGO-sandwiched SiNW@G nanocables (SiNW@G@RGO). Within this architecture, the overlapped G sheets act as adaptable but sealed sheaths to synergistically transform with the volume change of embedded SiNWs. This prevents the direct contact of silicon with the electrolyte, avoids the pore formation in silicon, and thus secures the integrity of SiNWs during repeated cycling. Moreover, the RGO overcoats, as a mechanically robust and flexible matrix, accommodate the volume change of embedded SiNW@G nanocables, thus maintaining the structural and electrical integrity of the electrode. That is to say, in a zoom-in view the thus-constructed SiNW@G@RGO is adaptable and can freely switch between a contracted state and an expanded state upon lithiation and delithiation (Figure 1). To the best of our knowledge, this is the first demonstration of a self-supporting binder-free Si–C anode prototype with silicon secured by dual adaptable apparels (sealed and open), which is significantly distinct from previously reported Si nanostructures encapsulated with either rigid/sealed or elastic/open coatings. Furthermore, this unique encapsulation of silicon has endowed the SiNW@G@RGO with much improved lithium storage performance when compared to their counterparts.

## RESULTS AND DISCUSSION

Briefly, the fabrication of SiNW@G@RGO is realized *via* vapor–liquid–solid (VLS) synthesis of SiNWs, chemical vapor deposition (CVD) growth of graphene on the

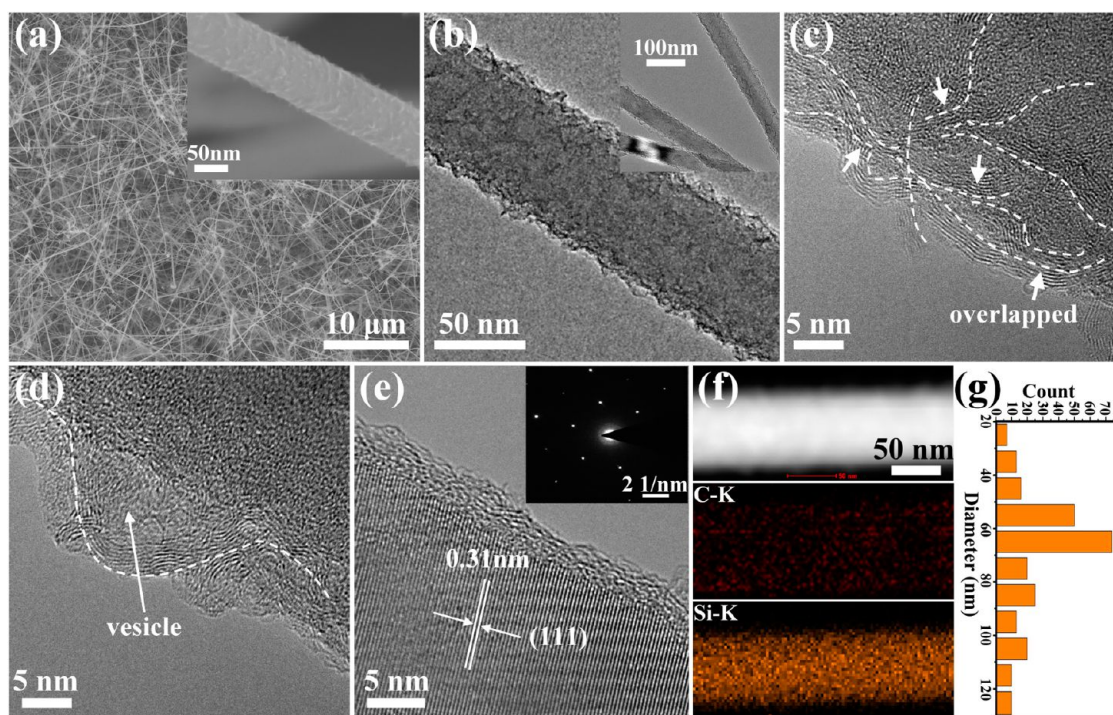


**Figure 2.** The structure and morphology of SiNW@G nanocables: (a) SEM image with an enlarged view in the inset; (b) TEM image with lower magnification view in the inset; (c–e) high resolution TEM images showing (c) overlapped, (d) vesicle-like, and (e) regular graphene sheets on the SiNW cores. The inset of panel e shows SAED pattern highlighting the crystalline structure of SiNW cores showing a [112] growth orientation. (f) Scanning transmission electron microscopy (STEM) and carbon and silicon elemental mapping images of individual SiNW@G nanocable; (g) diameter distribution of SiNW@G nanocables.

SiNWs to form SiNW@G nanocables, and vacuum filtration of an aqueous SiNW@G-graphene oxide (GO) dispersion followed by thermal reduction (see Methods for details). The structure and morphology of thus-synthesized SiNW@G nanocables were first characterized using scanning electron microscopy (SEM), transmission electron microscopy (TEM), and Raman spectroscopy (Figure 2 and Supporting Information, Figure S2). Different from the originally synthesized crystalline SiNWs with smooth surfaces (Supporting Information, Figure S1), the SiNW@G nanocables become quite textured (inset of Figure 2a) and show scale-like structures (Figure 2b), implying the successful coating of G sheaths on SiNWs. As turbostratic carbon may exist sparsely in the G sheaths, the high resolution TEM images further show that these G sheaths mainly consist of irregularly overlapped graphene sheets (Figure 2c) and void vesicle-like graphene sheets (Figure 2d), both of which are composed of few-layer graphene (typically, 5–8 layers) as verified by Raman results (Supporting Information, Figure S2). It should be mentioned that, in some areas graphene sheets are observed to lie in a regular manner on the surface of SiNWs, which facilitates the identification of the crystalline structure of SiNWs by selected area electron diffraction (SAED) (Figure 2e). Whereas these introduced graphene sheets bear different modalities and undulating features, the carbon and silicon elemental mapping (Figure 2f) displays a

highly homogeneous distribution of carbon on silicon, highlighting the uniform coating of G sheaths on SiNW cores. Furthermore, as shown in Figure 2g, the SiNW@G nanocables show an average diameter of about 65 nm, which is slightly larger than that for the pristine SiNWs (*ca.* 50 nm), attributable to the contribution of G sheaths (about 7.5 nm in thickness). Upon the combination of SiNW@G nanocables with GO (Supporting Information, Figure S3) followed by thermal reduction, the resulting paper-like SiNW@G@RGO films are self-supporting, flexible, and remain integral when being bent (Figure 3a). The cross-section SEM image of the film (Figure 3b) reveals that well-distributed SiNW@G nanocables are homogeneously sandwiched in between RGO sheets, forming a three-dimensional porous structure, which resembles the combination of one-dimensional carbon nanotubes and two-dimensional graphene.<sup>30</sup> The higher magnification cross-section and top-surface SEM images further manifest the intimate contact between the SiNW@G nanocables and adjacent RGO overcoats (inset of Figure 3b and Figure 3c). In addition, energy dispersive X-ray (EDX) analyses invariably disclose that the silicon content is about 60 wt % for many defined regions as exemplified by a white rectangle in Figure 3d, which is in good agreement with the weighting results (see Methods for details) and further indicates the uniform distribution of SiNW@G nanocables in the RGO matrix.

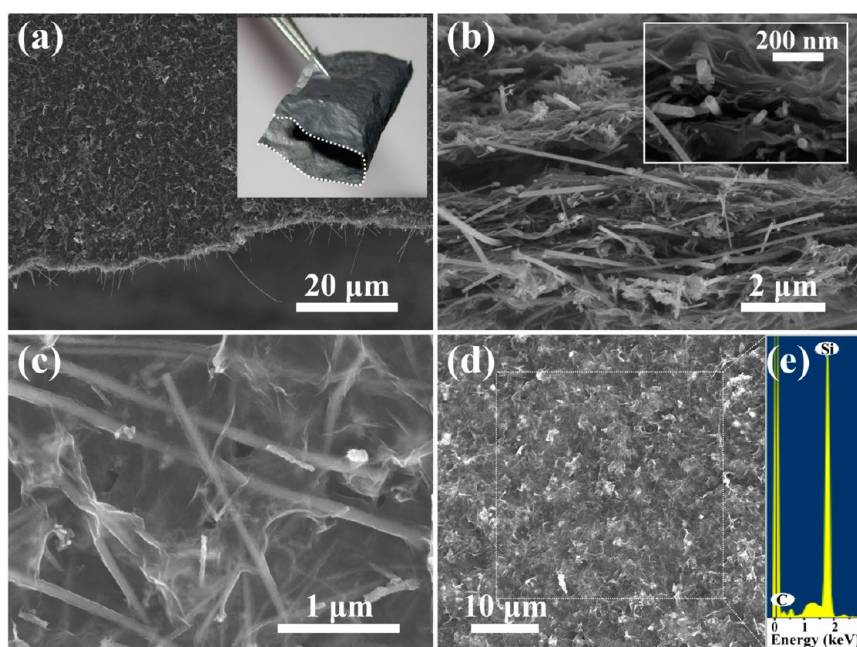


**Figure 3.** Characterization of SiNW@G@RGO: (a) low magnification SEM image. The inset shows an optical image of a bent SiNW@G@RGO film with a dashed line highlighting its edges. (b) Cross-section and (c) top-surface SEM images. The inset of panel b shows an enlarged cross-section view. (d) The corresponding region for collecting EDX spectrum in (e).

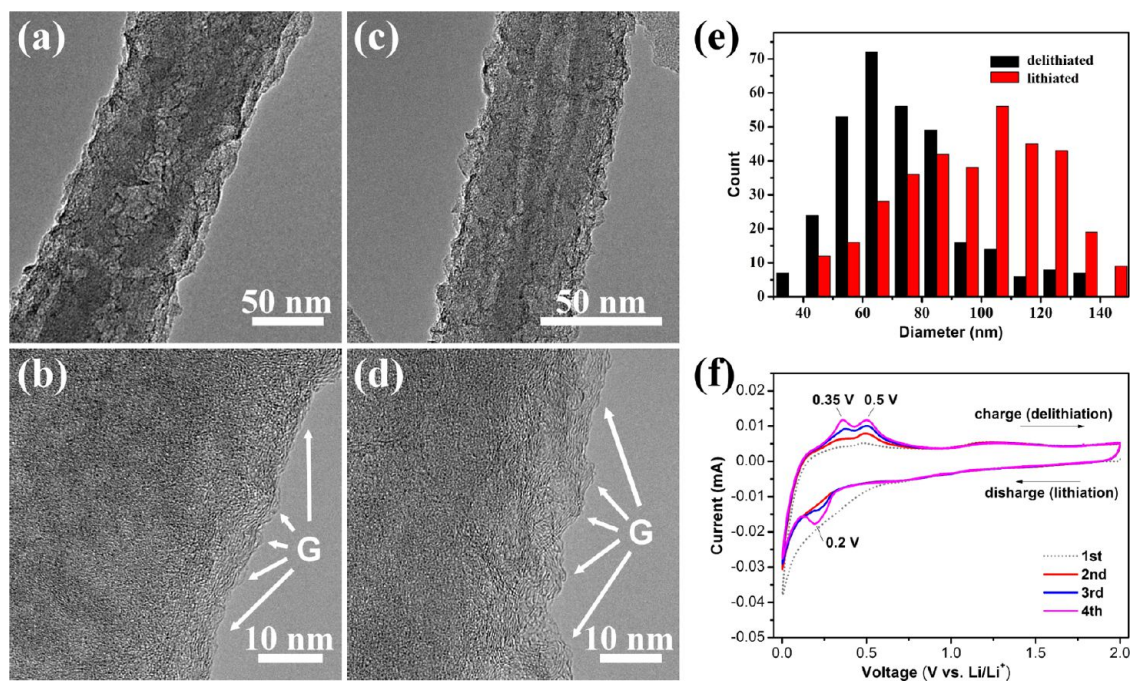


**Figure 4.** Characterization of the adapting process of SiNW@G@RGO: TEM images of SiNW@G nanocables from (a,b) almost fully lithiated and (c,d) delithiated SiNW@G@RGO electrodes at the third cycle; (e) statistical analysis of the diameters of lithiated and delithiated SiNW@G nanocables; (f) cyclic voltammetry curves of a SiNW@G@RGO electrode for the first four cycles.

To disclose that the as-synthesized SiNW@G@RGO material experiences adapting processes upon lithiation and delithiation (discharge/charge), we prepared battery half cells in which the SiNW@G@RGO was directly used as the working electrodes and paired with lithium foil counter electrodes. These SiNW@G@RGO electrodes were discharged and charged at a constant current of  $210 \text{ mA g}^{-1}$  and extracted for

observation with TEM (Figure 4). Hereof, most of SiNW@G nanocables were detached from RGO overcoats during the TEM sample preparation, which nevertheless facilitated the characterization of the structural and morphological changes of SiNW@G nanocables after lithiation and/or delithiation. Apparently, the silicon nanowire cores remain mostly amorphous in both lithiated and delithiated states, in accord

with those observed for crystalline Si after experiencing the first discharge, during which the Si reacts with lithium ions to form amorphous  $\text{Li}_x\text{Si}$ .<sup>3,31</sup> More importantly, corrugated graphene sheets comprising the G sheath are observed to remain on the amorphous nanowire surface, but the sheath becomes relatively smooth and flat after lithiation (Figure 4a,b), which in turn changes back to their originally rough and angular state after delithiation (Figure 4c,d). A statistical analysis shows that the average diameter of SiNW@G nanocables increases from 65 to 105 nm after lithiation (Figure 4e vs Figure 2g), which corresponds to approximately 260% volume expansion of the nanocable as well as more than 320% as for the silicon nanowire core alone, given that both the nanocable length and the sheath thickness are constant. Interestingly, the average diameter of SiNW@G nanocables returns back to their original value (*ca.* 65 nm) after delithiation although a slightly broader distribution profile of their diameters is observed in comparison with that of the pristine SiNW@G nanocables (Figure 4e vs Figure 2g). The above results clearly indicate that the G sheaths closely cooperate with interior SiNW cores and transform freely between an expanded state and a contracted state during cycling (Figure 1), indicating their adaptable essence. Similar to the confining effect of other mechanically rigid shells/sheaths on the silicon material, notably, the adaptable G sheaths also make the encapsulated silicon nanowires appear continuous and uniform even after many cycles (Figure 4c and Supporting Information, Figure S4), and remain intact. In contrast, a highly porous, sponge-like structure is generally observed after cycling for those SiNWs either uncovered<sup>32</sup> or sandwiched directly by RGO (Supporting Information, Figure S5). Taking into account the reported mechanisms<sup>3,33–37</sup> leading to the fracture and pore formation in silicon, the above results suggest two interesting points. First, the overlapped graphene sheets are loosely attached onto the SiNW surfaces possibly *via* a relatively weak interaction similar to those reported,<sup>38</sup> because a tight bonding (*e.g.*, covalent) between them can induce a strong confinement for expanded silicon and necessarily result in the fracture of silicon during lithiation.<sup>34–36</sup> Second, during repeated cycling the overlapped graphene sheets function as nearly sealed sheaths to prevent the direct exposure of silicon to the electrolyte and effectively alleviate SEI formation and propagation on silicon since the SEI formation can lead to the pore formation and propagation in silicon.<sup>34</sup> It is plausible that the G sheaths cannot track the huge circumferential change (about 60%) even though graphene is known to sustain a maximum strain of 10% without plastic deformations.<sup>39</sup> The adaptability of SiNW@G nanocables may originate from the initial sliding between overlapped graphene sheets during the first lithiation process as well as the subsequent contracting/expanding

deformation of the thus-expanded G sheaths during cycling. Furthermore, it should be noted that the RGO overcoats in the SiNW@G@RGO function as a flexible and adaptable matrix<sup>26–28</sup> to accommodate the contracting/expanding deformation of the sandwiched SiNW@G nanocables, which actually play a critically important role in guaranteeing the structural and electrical integrity of the electrodes upon cycling as demonstrated later.

Cyclic voltammetry (CV) was performed to further characterize the charge/discharge process of the SiNW@G@RGO in the voltage range of 2.0 V–0.002 V (*versus* Li/Li<sup>+</sup>) at a sweep rate of 0.1 mV s<sup>-1</sup> (Figure 4f). Resembling those reported for Si–C electrodes,<sup>40</sup> it is clear that the CV curve of the first cycle is quite different from those of subsequent cycles, especially for the discharge branch. In the first cycle the discharge current suddenly increases at a potential of around 0.7 V and becomes quite large below 0.3 V, which is usually ascribed to the occurrence of side reactions on the electrode surfaces and interfaces and to SEI formation,<sup>41–43</sup> as well as the lithiation of crystalline Si to form amorphous  $\text{Li}_x\text{Si}$ .<sup>44</sup> In comparison, the distinct peaks appear at 0.2 V during discharge and at 0.35 and 0.5 V during charge from the second cycle onward, exclusively representing the phase transformation between amorphous Si and  $\text{Li}_x\text{Si}$ , in accord with the above TEM observations and those previously reported in the literatures<sup>3,6,7</sup> for Si electrodes. Hereof, it is noteworthy that a thin and stable SEI film, formed on the surfaces and interfaces of overlapped graphene sheets in the first cycle, can rather consolidate<sup>15</sup> the role of G sheaths in preventing the direct contact of interior silicon nanowires with electrolyte and securing the structural integrity of interior silicon during subsequent charge–discharge cycles.

The dual encapsulation of silicon with adaptable apparels and consequent structural and interfacial stability of SiNW@G@RGO should afford excellent lithium storage performance even if without the addition of electrolyte additives<sup>7</sup> and/or the control of cutoff voltages<sup>45</sup> (Figure 5). Unless otherwise noted, the specific capacity values reported in Figure 5 are calculated on the basis of the total weight of SiNW@G@RGO, in which silicon comprises  $\sim$ 60% of the total mass. For comparison, the cycling performances of SiNW and SiNW@G electrodes (see Methods for their fabrication details) are exhibited in Figure 5a as well. It can be observed that the SiNW electrode shows very fast capacity fading and bears a negligible specific capacity value (*ca.* 50 mAh g<sup>-1</sup>) at the 50th cycle. After covering SiNWs with G sheaths, the cycling performance is slightly improved with 47% capacity retention (270 mAh g<sup>-1</sup>) at the 50th cycle, but still much poorer in comparison with those reported elsewhere.<sup>7</sup> This can be mainly due to the use of other components in the SiNW@G electrode, such as PVDF,<sup>23</sup>

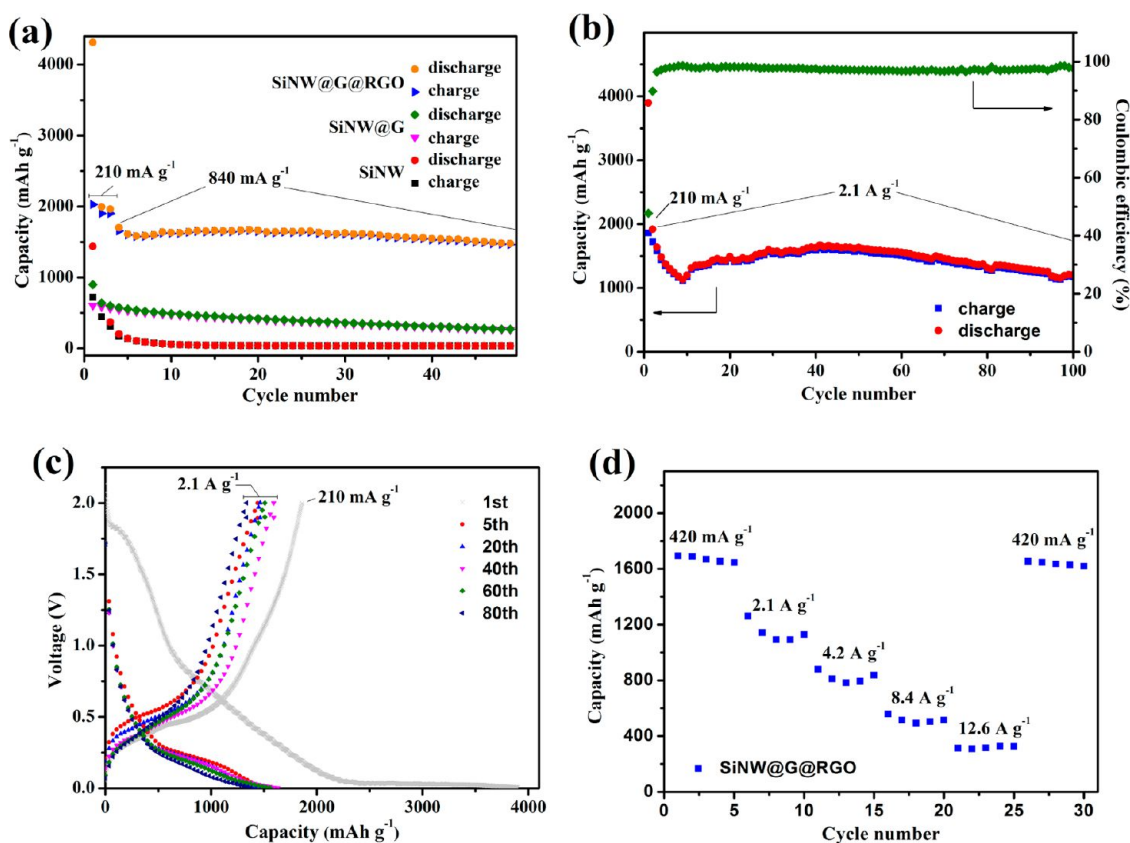


**Figure 5.** Electrochemical characteristics of SiNW@G@RGO. (a) Comparison of capacity retention of different electrodes. All electrodes were cycled at the charge/discharge rate of  $210 \text{ mA g}^{-1}$  for the first three cycles and then  $840 \text{ mA g}^{-1}$  for the subsequent cycles; (b) capacity and Coulombic efficiency of the SiNW@G@RGO cycled at the designated rate ( $210 \text{ mA g}^{-1}$  for the initial cycle and then  $2.1 \text{ A g}^{-1}$ ) for 100 cycles; (c) voltage profiles for different cycles in panel b; (d) charge (delithiation) capacities at various rates as marked. All the specific capacities reported and current densities used are based on the total electrode weight.

which fail to accommodate the spacing change between the SiNW@G nanocables and rapidly become ineffective in maintaining the structural integrity and electrical conductivity of the electrode. In contrast, after introducing two adaptable apparels (G and RGO), the self-supporting SiNW@G@RGO electrode delivers a significantly high specific capacity of about  $1650 \text{ mAh g}^{-1}$  at  $840 \text{ mA g}^{-1}$ , corresponding to a quite high specific capacity ( $2750 \text{ mAh g}^{-1}$ ) for silicon alone, which remains almost constant over the 50 cycles investigated. The long-term cycling stability of SiNW@G@RGO was further studied at  $210 \text{ mA g}^{-1}$  in the first two cycles and then at  $2.1 \text{ A g}^{-1}$  in the subsequent 100 cycles (Figure 5b). Surprisingly, the specific capacity can reach approximately  $1600 \text{ mAh g}^{-1}$  at the rate of  $2.1 \text{ A g}^{-1}$  and retains approximately 80% of its initial capacity after 100 cycles. The significantly high specific capacity and superior capacity retention achieved at such a large rate ( $2.1 \text{ A g}^{-1}$ ), on the basis of the total electrode weight, can be attributed to the unique architecture of the SiNW@G@RGO electrodes. It should be pointed out that the Coulombic efficiency of the first cycle is relatively low ( $\sim 50\%$ ) in this study, which can be due to the consumption of lithium by the

defects on G and RGO, as well as initial SEI formation. It is very possible to avoid this drawback by interfacial treatments, electrolyte modifications,<sup>7</sup> and/or material prelithiation<sup>45</sup> in future studies. From the third cycle onward the SiNW@G@RGO electrodes demonstrate Coulombic efficiencies of more than 98% (Figure 5b). The voltage profiles of different cycles are shown in Figure 5c. While the first charge–discharge cycle usually involves the SEI formation and the transformation of crystalline Si into amorphous Si as discussed above, the voltage profiles are very similar from the second cycle onward, which are in good agreement with the behavior of amorphous silicon, although both G sheaths and RGO overcoats contribute to them. No obvious change in both charge and discharge profiles is observed even after 100 cycles, which further indicates that the silicon nanowires with dual breathable adaptable apparels are extraordinarily stable during cycling. In addition, the dual encapsulation also endows the SiNW@G@RGO electrodes with superior rate capability (Figure 5d). Under fast ( $8.4 \text{ A g}^{-1}$ ) and deep ( $2 - 0.002 \text{ V}$ ) discharge/charge cycling, a high charge (delithiation) capacity of *ca.*  $500 \text{ mAh g}^{-1}$  can be obtained on the basis of the total electrode weight;

Even after cycling at very high current rates (e.g.,  $12.6 \text{ A g}^{-1}$ ), the capacity is still recoverable as validated by the case at  $420 \text{ mA g}^{-1}$ .

Both high reversible capacity and outstanding capacity retention of SiNW@G@RGO substantiate that such a dual encapsulation formula allows one to stabilize silicon-based anodes, and this may be attributed to the following aspects: first, the G sheaths of SiNW@G nanocables are highly adaptable, being capable of synchronous deformation on the heels of the dramatic volume change of SiNWs instead of being cracked during cycling. This effectively prevents the direct contact between silicon nanowires and electrolyte during cycling, thus alleviating the formation and propagation of the SEI layer and also inhibiting the pore formation in silicon. Second, the RGO overcoats are highly flexible, holding the intrinsic ability to accommodate the volume change of SiNW@G nanocables, thus maintaining the structural integrity of the electrode. Third, although being well dispersed in the RGO, silicon nanowires located between the same two RGO overcoats may be displaced and fused together<sup>35,46</sup> during charge–discharge processes given the absence of G sheaths, thus impairing the nanostructure effect and causing capacity fading to occur. In contrast, the G sheaths here-introduced can isolate each silicon nanowire from others and guarantee each silicon nanowire counted to function separately and efficiently. Fourth, the G sheaths of SiNW@G nanocables, are interconnected through surrounding RGO overcoats, thus forming a quite effective and continuous conductive network. More importantly, the lateral contact between SiNW cores and their dual apparels (G and RGO) greatly shortens the electron transport distance from/to silicon, and is thus highly favorable for improving their rate capability, which is clearly different from the axial transport in the SiNWs deposited directly on metal current collectors.<sup>3</sup> Fifth, the dimensional hybridization present in SiNW@G@RGO enables the formation of a three-dimensional porous network,

thus significantly facilitating the diffusion and transport of lithium ions even at high current rates. Sixth, both G and RGO may contribute to the capacity of the electrode. Last, thanks to the flexible nature of G and RGO, the resulting SiNW@G@RGO material is robust and free-standing, thus avoiding the necessity of additional additives (e.g., traditional binders) that may degrade the performance of as-designed anode materials, for example by disturbing their structural integrity and continuity.

## CONCLUSION

We have successfully fabricated a novel kind of self-supporting binder-free silicon-based anodes *via* the encapsulation of silicon nanowires with overlapped graphene sheets (G sheaths) and RGO overcoats. In the architecture, the overlapped graphene sheets, as adaptable but sealed sheaths, synergistically transform with the volume change of embedded silicon, thus effectively preventing the direct exposure of encapsulated silicon to the electrolyte and enabling the structural and interfacial stabilization of encapsulated silicon nanowires during cycling. Meanwhile, the flexible and conductive RGO overcoats accommodate the volume change of embedded SiNW@G nanocables, maintaining the structural and electrical integrity of the electrode. As a result, the electrodes exhibit outstanding lithium storage performance with high reversible specific capacity of  $1600 \text{ mAh g}^{-1}$  at  $2.1 \text{ A g}^{-1}$ , 80% capacity retention after 100 cycles, and superior rate capability ( $500 \text{ mAh g}^{-1}$  at  $8.4 \text{ A g}^{-1}$ ) on the basis of the total electrode weight. While further improvement of these performance parameters may be possible on the basis of the modification and optimization of the components and interfaces of SiNW@G@RGO, the strategy to encapsulate silicon with dual (sealed/open) adaptable matrices demonstrated here opens up a new avenue for developing high-performance silicon-based anodes, and can be also extended to other fascinating anode and cathode materials systems that undergo large volume expansion.

## METHODS

**Materials.** The procedure for making SiNW@G@RGO contains the synthesis of silicon nanowires (SiNWs), the sheathing of SiNWs with overlapped graphene sheets to form silicon nanowire/overlapped graphene sheet core–sheath nanocables (SiNW@G), and the sandwiching of SiNW@G nanocables with reduced graphene oxide (RGO). In detail, the SiNWs with an average diameter of about 50 nm and a typical length of more than  $50 \mu\text{m}$  were first grown *via* a chemical vapor deposition (CVD) vapor–liquid–solid (VLS) growth method as reported elsewhere.<sup>47</sup> Briefly, the SiNWs were grown by passing 300 standard cubic centimeters (sccm) of silane ( $\text{SiH}_4$ , 50% diluted with hydrogen) at a pressure of 3 Torr across a Si substrate containing Au catalyst. The typical deposition temperature and time was  $500 \text{ }^\circ\text{C}$  and 30 min. The as-prepared SiNWs were immersed in gold etchant solution to remove Au catalyst particles, and then collected and placed in a quartz boat, which

was heated to  $1050 \text{ }^\circ\text{C}$  in a horizontal tube furnace under argon/hydrogen ( $\text{Ar}/\text{H}_2$ ; 2:1) atmosphere. Then, 50 sccm  $\text{CH}_4$  was introduced into the reaction tube and kept for 5 min. After that, the sample was rapidly cooled to room temperature under the protection of Ar and  $\text{H}_2$ , thus obtaining SiNW@G nanocables. Finally, the SiNW@G nanocables were well dispersed in graphene oxide (GO) solution with a desirable concentration (typically,  $0.1 \text{ mg/mL}$ ) which was made on the basis of the modified Hummers method.<sup>48</sup> The homogeneous mixture obtained was vacuum filtered and peeled from the filter membrane to get the flexible paper-like composite cake, which was further annealed at  $600 \text{ }^\circ\text{C}$  for 2 h under Ar, thus obtaining reduced graphene oxide (RGO)-sandwiched SiNW@G nanocables (namely, SiNW@G@RGO). The weight ratio of silicon in the SiNW@G@RGO material was determined by measuring the weight increment five consecutive times after each processing step using a high-precision electronic balance, as well as averaging the values from more than five samples. For some control

experiments, the originally synthesized SiNWs were also sandwiched directly with RGO *via* the above vacuum filtration process followed by thermal annealing.

**Characterization.** The structure and morphology of the samples were investigated by FE-SEM (Hitachi S4800) and FE-TEM (FEI Tecnai G2 20 STWIN and Tecnai G2 F20 U-TWIN). Raman spectra were collected using a Renishaw inVia Raman microscope with a laser wavelength of 514.5 nm. For electrochemical measurements, both SiNW and SiNW@G working electrodes were prepared by mixing the active material (SiNWs and SiNW@G nanocables, respectively) with super P carbon black and polyvinylidene fluoride (PVDF) binder in *N*-methyl-2-pyrrolidone (NMP) at a weight ratio of 6:2:2, and then casting on current collectors (copper foil). Different from that in the above fabrication procedure, the paper-like SiNW@G@RGO material was directly used as the working electrode. The as-made working electrodes were assembled into coin-type half cells (CR2032) in an argon-filled glovebox with lithium foil as the counter electrode, porous polypropylene film as the separator, and 1 M LiPF<sub>6</sub> in 1:1 (v/v) ethylene carbonate/diethyl carbonate (EC/DEC) as the electrolyte. The cycle-life tests were performed using a CT2001A battery program controlling test system at different current rates within the 2–0.002 V voltage range. For each investigated working electrode, the total electrode weight was used for setting current densities and calculating specific capacities. Cyclic voltammetry was performed with a CHI660D electrochemical station in the voltage range of 2.0–0.002 V (versus Li/Li<sup>+</sup>) at a sweep rate of 0.1 mV s<sup>-1</sup>. In some cases the cells were fully charged and/or discharged, and then disassembled and washed completely with NMP, dilute HCl, and ethanol for TEM analysis, a technique based on a washing process reported elsewhere.<sup>19</sup>

**Conflict of Interest:** The authors declare no competing financial interest.

**Supporting Information Available:** Figure S1–S5 as described in the text. This material is available free of charge *via* the Internet at <http://pubs.acs.org>.

**Acknowledgment.** Financial support from the National Natural Science Foundation of China (Grant Nos. 20973044, 21173057, 21273054), the Ministry of Science and Technology of China (No. 2012CB933400 and No. 2012CB933403), the Chinese Academy of Sciences, and Beijing Municipal Science and Technology Commission is acknowledged. S.T.P. also acknowledges support from Nanostructures for Electrical Energy Storage, an Energy Frontier Research Center funded by the U.S. Department of Energy, Office of Science, Office of Basic Energy Sciences under Award Number DESC0001160.

## REFERENCES AND NOTES

- Tarascon, J.-M.; Armand, M. Issues and Challenges Facing Rechargeable Lithium Batteries. *Nature* **2001**, *414*, 359–367.
- Armand, M.; Tarascon, J.-M. Building Better Batteries. *Nature* **2008**, *451*, 652–657.
- Chan, C. K.; Peng, H.; Liu, G.; McIlwrath, K.; Zhang, X. F.; Huggins, R. A.; Cui, Y. High-Performance Lithium Battery Anodes Using Silicon Nanowires. *Nat. Nanotechnol.* **2008**, *3*, 31–35.
- Magasinski, A.; Dixon, P.; Hertzberg, B.; Kvit, A.; Ayala, J.; Yushin, G. High-Performance Lithium-Ion Anodes Using a Hierarchical Bottom-up Approach. *Nat. Mater.* **2010**, *9*, 353–358.
- Wu, H.; Chan, G.; Choi, J. W.; Ryu, I.; Yao, Y.; McDowell, M. T.; Lee, S. W.; Jackson, A.; Yang, Y.; Hu, L.; *et al.* Stable Cycling of Double-Walled Silicon Nanotube Battery Anodes through Solid-Electrolyte Interphase Control. *Nat. Nanotechnol.* **2012**, *7*, 310–315.
- Kasavajula, U.; Wang, C.; Appleby, A. J. Nano- and Bulk-Silicon-Based Insertion Anodes for Lithium-Ion Secondary Cells. *J. Power Sources* **2007**, *163*, 1003–1039.
- Szczeczek, J. R.; Jin, S. Nanostructured Silicon for High Capacity Lithium Battery Anodes. *Energy Environ. Sci.* **2011**, *4*, 56–72.
- Kim, H.; Seo, M.; Park, M.-H.; Cho, J. A Critical Size of Silicon Nano-anodes for Lithium Rechargeable Batteries. *Angew. Chem., Int. Ed.* **2010**, *49*, 2146–2149.
- Liu, X. H.; Zhong, L.; Huang, S.; Mao, S. X.; Zhu, T.; Huang, J. Y. Size-Dependent Fracture of Silicon Nanoparticles During Lithiation. *ACS Nano* **2012**, *6*, 1522–1531.
- Kim, H.; Cho, J. Superior Lithium Electroactive Mesoporous Si@Carbon Core–Shell Nanowires for Lithium Battery Anode Material. *Nano Lett.* **2008**, *8*, 3688–3691.
- Park, M.-H.; Kim, M. G.; Joo, J.; Kim, K.; Kim, J.; Ahn, S.; Cui, Y.; Cho, J. Silicon Nanotube Battery Anodes. *Nano Lett.* **2009**, *9*, 3844–3847.
- Hertzberg, B.; Alexeev, A.; Yushin, G. Deformations in Si–Li Anodes upon Electrochemical Alloying in Nano-confined Space. *J. Am. Chem. Soc.* **2010**, *132*, 8548–8549.
- Ng, S.-H.; Wang, J.; Wexler, D.; Konstantinov, K.; Guo, Z. P.; Liu, H. K. Highly Reversible Lithium Storage in Spheroidal Carbon-Coated Silicon Nanocomposites as Anodes for Lithium-Ion Batteries. *Angew. Chem., Int. Ed.* **2006**, *45*, 6896–6899.
- Kim, H.; Han, B.; Choo, J.; Cho, J. Three-Dimensional Porous Silicon Particles for Use in High-Performance Lithium Secondary Batteries. *Angew. Chem., Int. Ed.* **2008**, *47*, 10151–10154.
- Liu, N.; Wu, H.; McDowell, M. T.; Yao, Y.; Wang, C.; Cui, Y. A Yolk–Shell Design for Stabilized and Scalable Li-Ion Battery Alloy Anodes. *Nano Lett.* **2012**, *12*, 3315–3321.
- Cho, Y. J.; Kim, H. S.; Im, H.; Myung, Y.; Jung, G. B.; Lee, C. W.; Park, J.; Park, M.-H.; Cho, J.; Kang, H. S. Nitrogen-Doped Graphitic Layers Deposited on Silicon Nanowires for Efficient Lithium-Ion Battery Anodes. *J. Phys. Chem. C* **2011**, *115*, 9451–9457.
- Yao, Y.; Liu, N.; McDowell, M. T.; Pasta, M.; Cui, Y. Improving the Cycling Stability of Silicon Nanowire Anodes with Conducting Polymer Coatings. *Energy Environ. Sci.* **2012**, *5*, 7927–7930.
- Hwang, T. H.; Lee, Y. M.; Kong, B.-S.; Seo, J.-S.; Choi, J. W. Electrospun Core–Shell Fibers for Robust Silicon Nanoparticle-Based Lithium Ion Battery Anodes. *Nano Lett.* **2012**, *12*, 802–807.
- Wu, H.; Zheng, G.; Liu, N.; Carney, T. J.; Yang, Y.; Cui, Y. Engineering Empty Space between Si Nanoparticles for Lithium-Ion Battery Anodes. *Nano Lett.* **2012**, *12*, 904–909.
- Hu, Y.-S.; Demir-Cakan, R.; Titirici, M.-M.; Muller, J.-O.; Schlogl, R.; Antonietti, M.; Maier, J. Superior Storage Performance of a Si@SiO<sub>2</sub>/C Nanocomposite as Anode Material for Lithium-Ion Batteries. *Angew. Chem., Int. Ed.* **2008**, *47*, 1645–1649.
- Su, L.; Zhou, Z.; Ren, M. Core Double-Shell Si@SiO<sub>2</sub>@C Nanocomposites as Anode Materials for Li-Ion Batteries. *Chem. Commun.* **2010**, *46*, 2590–2592.
- Cao, F. F.; Deng, J.-W.; Xin, S.; Ji, H.-X.; Schmidt, O. G.; Wan, L.-J.; Guo, Y.-G. Cu–Si Nanocable Arrays as High-Rate Anode Materials for Lithium-Ion Batteries. *Adv. Mater.* **2011**, *23*, 4415–4420.
- Kovalenko, I.; Zdyrko, B.; Magasinski, A.; Hertzberg, B.; Milicev, Z.; Burtovyy, R.; Luzinov, I.; Yushin, G. A Major Constituent of Brown Algae for Use in High-Capacity Li-Ion Batteries. *Science* **2011**, *334*, 75–79.
- Li, X.; Cho, J.-H.; Li, N.; Zhang, Y.; Williams, D.; Dayeh, S. A.; Picraux, S. T. Carbon Nanotube-Enhanced Growth of Silicon Nanowires as an Anode for High-Performance Lithium-Ion Batteries. *Adv. Energy Mater.* **2012**, *2*, 87–93.
- Geim, A. K. Random Walk to Graphene (Nobel Lecture). *Angew. Chem., Int. Ed.* **2011**, *50*, 6966–6985.
- Wu, D.; Zhang, F.; Liu, P.; Feng, X. Two-Dimensional Nanocomposites Based on Chemically Modified Graphene. *Chem.—Eur. J.* **2011**, *17*, 10804–10812.
- Lee, J. K.; Smith, K. B.; Hayner, C. M.; Kung, H. H. Silicon Nanoparticles-Graphene Paper Composites for Li Ion Battery Anodes. *Chem. Commun.* **2010**, *46*, 2025–2027.
- Wang, J.-Z.; Zhong, C.; Chou, S.-L.; Liu, H.-K. Flexible Free-Standing Graphene-Silicon Composite Film for Lithium-Ion Batteries. *Electrochem. Commun.* **2010**, *12*, 1467–1470.
- Yang, P.; Tarascon, J.-M. Towards Systems Materials Engineering. *Nat. Mater.* **2012**, *11*, 560–563.

30. Fan, Z.; Yan, J.; Zhi, L.; Zhang, Q.; Wei, T.; Feng, J.; Zhang, M.; Qian, W.; Wei, F. A Three-Dimensional Carbon Nanotube/Graphene Sandwich and Its Application as Electrode in Supercapacitors. *Adv. Mater.* **2010**, *22*, 3723–3728.
31. Liu, X. H.; Zhang, L. Q.; Zhong, L.; Liu, Y.; Zheng, H.; Wang, J. W.; Cho, J.-H.; Dayeh, S. A.; Picraux, S. T.; Sullivan, J. P.; *et al.* Ultrafast Electrochemical Lithiation of Individual Si Nanowire Anodes. *Nano Lett.* **2011**, *11*, 2251–2258.
32. Choi, J. W.; McDonough, J.; Jeong, S.; Yoo, J. S.; Chan, C. K.; Cui, Y. Stepwise Nanopore Evolution in One-Dimensional Nanostructures. *Nano Lett.* **2010**, *10*, 1409–1413.
33. Liu, X. H.; Zheng, H.; Zhong, L.; Huang, S.; Karki, K.; Zhang, L. Q.; Liu, Y.; Kushima, A.; Liang, W. T.; Wang, J. W.; *et al.* Anisotropic Swelling and Fracture of Silicon Nanowires during Lithiation. *Nano Lett.* **2011**, *11*, 3312–3318.
34. Hu, L.; Wu, H.; Gao, Y.; Cao, A.; Li, H.; McDough, J.; Xie, X.; Zhou, M.; Cui, Y. Silicon-Carbon Nanotube Coaxial Sponge as Li-Ion Anodes with High Areal Capacity. *Adv. Energy Mater.* **2011**, *1*, 523–527.
35. Gu, M.; Li, Y.; Li, X.; Hu, S.; Zhang, X.; Xu, W.; Thevuthasan, S.; Baer, D. R.; Zhang, J.-G.; Liu, J.; *et al.* *In Situ* TEM Study of Lithiation Behavior of Silicon Nanoparticles Attached to and Embedded in a Carbon Matrix. *ACS Nano* **2012**, *6*, 8439–8447.
36. Zhao, K. J.; Pharr, M.; Wan, Q.; Wang, W. L.; Kaxiras, E.; Vlassak, J. J.; Suo, Z. G. Concurrent Reaction and Plasticity During Initial Lithiation of Crystalline Silicon in Lithium-Ion Batteries. *J. Electrochem. Soc.* **2012**, *159*, A238–A243.
37. McDowell, M. T.; Ryu, I.; Lee, S. W.; Wang, C.; Nix, W. D.; Cui, Y. Studying the Kinetics of Crystalline Silicon Nanoparticle Lithiation with *in Situ* Transmission Electron Microscopy. *Adv. Mater.* **2012**, *24*, 6034–6041.
38. Kong, L.; Bjelkevig, C.; Gaddam, S.; Zhou, M.; Lee, Y. H.; Han, G. H.; Jeong, H. K.; Wu, N.; Zhang, Z.; Xiao, J.; *et al.* Graphene/Substrate Charge Transfer Characterized by Inverse Photoelectron Spectroscopy. *J. Phys. Chem. C* **2010**, *114*, 21618–21624.
39. Booth, T. J.; Blake, P.; Nair, R. R.; Jiang, D.; Hill, E. W.; Bangert, U.; Bleloch, A.; Gass, M.; Novoselov, K. S.; Katsnelson, M. I.; *et al.* Macroscopic Graphene Membranes and Their Extraordinary Stiffness. *Nano Lett.* **2008**, *8*, 2442–2446.
40. Huang, R.; Fan, X.; Shen, W.; Zhu, J. Carbon-Coated Silicon Nanowire Array Films for High-Performance Lithium-Ion Battery Anodes. *Appl. Phys. Lett.* **2009**, *95*, 133119.
41. Fong, R.; Sacken, U.; Dahn, J. R. Studies of Lithium Intercalation into Carbons Using Nonaqueous Electrochemical Cells. *J. Electrochem. Soc.* **1990**, *137*, 2009–2013.
42. Xing, W.; Dahn, J. R. Study of Irreversible Capacities for Li Insertion in Hard and Graphitic Carbons. *J. Electrochem. Soc.* **1997**, *144*, 1195–1201.
43. Graetz, J.; Ahn, C. C.; Yazami, R.; Fultz, B. Highly Reversible Lithium Storage in Nanostructured Silicon. *Electrochem. Solid-State Lett.* **2003**, *6*, A194–A197.
44. Wang, W.; Kumta, P. N. Nanostructured Hybrid Silicon/Carbon Nanotube Heterostructures: Reversible High-Capacity Lithium-Ion Anodes. *ACS Nano* **2010**, *4*, 2233–2241.
45. Liu, N.; Hu, L.; McDowell, M. T.; Jackson, A.; Cui, Y. Pre-lithiated Silicon Nanowires as an Anode for Lithium Ion Batteries. *ACS Nano* **2011**, *5*, 6487–6493.
46. Karki, K.; Epstein, E.; Cho, J.-H.; Jia, Z.; Li, T.; Picraux, S. T.; Wang, C.; Cumings, J. Lithium-Assisted Electrochemical Welding in Silicon Nanowire Battery Electrodes. *Nano Lett.* **2012**, *12*, 1392–1397.
47. Picraux, S. T.; Dayeh, S. A.; Manandhar, P.; Perea, D. E.; Choi, S. G. Silicon and Germanium Nanowires: Growth, Properties, and Integration. *JOM* **2010**, *62*, 35–43.
48. Hummers, W. S.; Offeman, R. E. Preparation of Graphitic Oxide. *J. Am. Chem. Soc.* **1958**, *80*, 1339–1339.